A Study of Fluctuations in Magnetic Cloud-Driven Sheaths

C. Moissard, D. Fontaine, P. Savoini

JGR Space Physics

RESEARCH ARTICLE
10.1029/2019JA026952

A Study of Fluctuations in Magnetic Cloud-Driven Sheaths

C. Moissard[1], D. Fontaine[1], and P. Savoini[1]

[1]LPP, CNRS, Ecole Polytechnique, Sorbonne Université, Université Paris Sud, Observatoire de Paris, Université Paris-Saclay, PSL Research University, Palaiseau, France

Key Points:
- The fluctuations in sheaths have increased power (∼10 times) and compressibility (∼2 times) compared to the solar wind's
- Those characteristics depend on magnetic clouds' speed, preexisting fluctuations in the solar wind, and shock's parameters

Correspondence to:
C. Moissard,
clement.moissard@lpp.polytechnique.fr

Citation:
Moissard, C., Fontaine, D., & Savoini, P. (2019). A study of fluctuations in magnetic cloud-driven sheaths. *Journal of Geophysical Research: Space Physics*, *124*, 8208–8226. https://doi.org/10.1029/2019JA026952

Received 16 MAY 2019
Accepted 2 SEP 2019
Accepted article online 16 OCT 2019
Published online 7 NOV 2019

Abstract Interplanetary coronal mass ejections are at the center of the research on geomagnetic activity. Sheaths, highly fluctuating structures, which can be found in front of fast interplanetary coronal mass ejections, are some of the least known geoeffective solar transients. Using Morlet transforms, we analyzed the magnetic fluctuations in a list of 42 well-identified and isolated magnetic clouds driving a sheath and shock (Masías-Meza et al., 2016, https://doi.org/10.1051/0004-6361/201628571. We studied the fluctuations inside sheaths by defining two quantities: the power and the anisotropy. With a simple statistical approach we found that sheaths, in particular, those driven by a fast magnetic cloud, encountering a highly turbulent solar wind, and forming a high Alfvén Mach number shock have high levels of turbulent energy (∼10 times compared with the solar wind) as well as a low anisotropy (approximately halved compared with the solar wind) of their fluctuations. On the other hand, the effect of the shock angle and plasma beta in the solar wind are less straightforward: If the shock is quasi-parallel or the beta in the solar wind is high, both the turbulent energy in the sheaths and the anisotropy of the fluctuations are reduced; but for quasi-perpendicular shocks or low beta solar wind the turbulent energy and anisotropy can take any value.

Plain Language Summary Solar flares are sometimes linked with the emission of interplanetary structures, which may collide with Earth. When this happens, it can lead to temporary changes in the magnetic field of Earth and possibly affect human technology. These effects are a subset of what is known as *geoeffectiveness*. We do have an idea of which types of structures may or may not have consequences on Earth, and, for example, *magnetic clouds* are quite well known for their large impact on the Earth magnetic field; however, we still struggle to understand the consequences of some puzzling interplanetary structures called *sheaths*. These can often be found preceding a magnetic cloud when the latter is fast enough to generate a shock wave. We think that one of the reasons these sheaths keep having surprising effects on the Earth's magnetic field is because they, themselves, are not yet very well known. The present paper aims at characterizing one of the key properties of sheaths: their *magnetic fluctuations*, that is, the rapid temporal variation of the magnetic field. We found that those *fluctuations* are indeed quite particular in sheaths: They have markedly more energy than in the usual solar wind (about 10 times more) and tend to change direction all the time. Conversely, in the solar wind, some directions seem to be privileged and the energy is relatively low. In this paper, we also show that these particular properties of the magnetic fluctuations are all the more pronounced when the magnetic cloud driving the sheath is moving faster and when the solar wind in front of the sheath already has strong fluctuations and magnetic pressure. This work gives us a better insight into the dynamics of the sheath, which may eventually improve our understanding of their geoeffectiveness.

1. Introduction

It has been extensively shown in the literature that magnetic clouds are the most geoeffective transient structures found in the solar wind (Kilpua et al., 2017; Wilson, 1987; Yermolaev et al., 2012; G. Zhang & Burlaga, 1988). This stems from the high probability of a magnetic cloud to present a long-lasting negative B_z component (Burlaga, 1991), which is a well-documented cause of geomagnetic storms (Dungey, 1961; Gonzalez & Tsurutani, 1987; Gonzalez et al., 1994; Kilpua et al., 2012; Russell et al., 1974; Tsurutani et al., 1992; Zhang & Moldwin, 2014), the explanation being that it favors magnetic reconnection at the nose of the magnetopause (Dungey, 1961; Gonzalez et al., 1989; Turc et al., 2014). However, this is not enough, as

magnetic storms on Earth are not all caused by magnetic clouds, and not all magnetic clouds cause magnetic storms.

When a magnetic cloud has a velocity higher than the characteristic speeds (sound speed or Alfvén speed) of the solar wind in which it is traveling, its interaction with the solar wind is likely to form a shock wave propagating away from the Sun. Between the shock front and the leading edge of the cloud we find a sheath, which is a highly turbulent region (Kilpua et al., 2017). Huttunen and Koskinen (2004) have shown that, between 1997 and 2002, 45% of the 53 intense (as defined by the geomagnetic index $Dst < -100$ nT) magnetic storms observed on Earth were caused by a turbulent sheath region or postshock stream, thus exposing in a particularly convincing way the important role played by interplanetary coronal mass ejection (ICME) sheaths but pointing out the fact that it is not always possible to separate their effect from the ICMEs following them, when there is one. More than half of the magnetic clouds are accompanied by a sheath (Chi et al., 2016), and the role of these sheaths is increasingly regarded as important (Echer et al., 2008; Kilpua et al., 2017; Tsurutani et al., 1988). For example, out of the 73 solar storms (defined by $Dst < -50$ nT) of Solar Cycle 23 (1997 to 2005), Huttunen et al. (2005) identified eight events—composed of both a magnetic cloud and a sheath—where the magnetic storm was clearly caused by the sheath and not the magnetic cloud. Gonzalez et al. (2007) found similar results studying Solar Cycle 23: Sheaths were responsible for the generation of 24% of the intense storms ($Dst < -100$ nT) during the cycle, and magnetic clouds accompanied by a sheath for 14%.

The reasons that may lead to the geoeffectiveness of sheaths are still unclear. Tsurutani et al. (1990) emphasized the high probability of a sheath to include southward magnetic field due to the numerous large-amplitude turnings of the magnetic field. The geoeffectiveness of sheaths has also been suggested to be linked to their most obvious traits: high density, high dynamic pressure, high magnetic field, high variability of the magnetic field (Yermolaev et al., 2012), or high Alfvén Mach number (Guo et al., 2011; Kilpua et al., 2017; Myllys et al., 2016). These traits, especially the high dynamic pressure, high level of fluctuations of the magnetic field, and high Alfvén Mach number, are known to increase solar wind-magnetosphere coupling (Kilpua et al., 2017).

Another visible trait of sheaths is their turbulence. Their internal structure, however, is still mostly unknown, and the role it plays in their geoeffectiveness could be underestimated. Indeed, it is known that the turbulence in the solar wind plays a role in the efficiency of its coupling with the magnetosphere: For example, Tsurutani et al. (1988) noted that, surprisingly, some major storms seem to be caused by something else than a long-lasting southward magnetic field and pointed at turbulence, waves, and discontinuities as drivers of geomagnetic activity; Borovsky (2003) showed correlations between the amplitude of turbulence in the solar wind and different geomagnetic activity indices; Jankovičvá et al. (2008) did a similar study with similar conclusions and introduced the anisotropy of the fluctuations in the discussion; Osmane et al. (2015) compared the ultralow frequency (ULF) fluctuations of the interplanetary magnetic field and the *AL* index (amplitude lower for the auroral electrojet index) and concluded that, by enhancing viscous interaction between the solar wind and the magnetosphere, fluctuations can drive geomagnetic activity. Those studies, which strongly link the level of turbulence in the solar wind in general with geoeffectiveness, suggest that the turbulence in sheaths may play a major part in geoeffectiveness.

Before even considering geoeffectiveness, more information is needed to uncover as much as possible about the waves and fluctuations in sheaths. Only a few studies have been performed on the subject. For example, Kataoka et al. (2005) evidenced the importance of the shock parameters in influencing the structure of the sheaths of ICMEs. Kilpua et al. (2013) showed that the power of the ULF waves evolved within sheaths with respect to the distance with the shock and the leading edge of the magnetic cloud. Shaikh et al. (2017) found in two cases that sheaths were home not only to turbulence but also to ordered local structures such as magnetic islands, which are strong candidates to explain multisteps Forbush decreases (a rapid decrease of the detected galactic cosmic rays). And recently, a statistical study by Ala-Lahti et al. (2018) suggested that, in sheaths, mirror modes could stem from the shock compression, making the Alfvénic Mach number the key parameter governing the structure of sheaths.

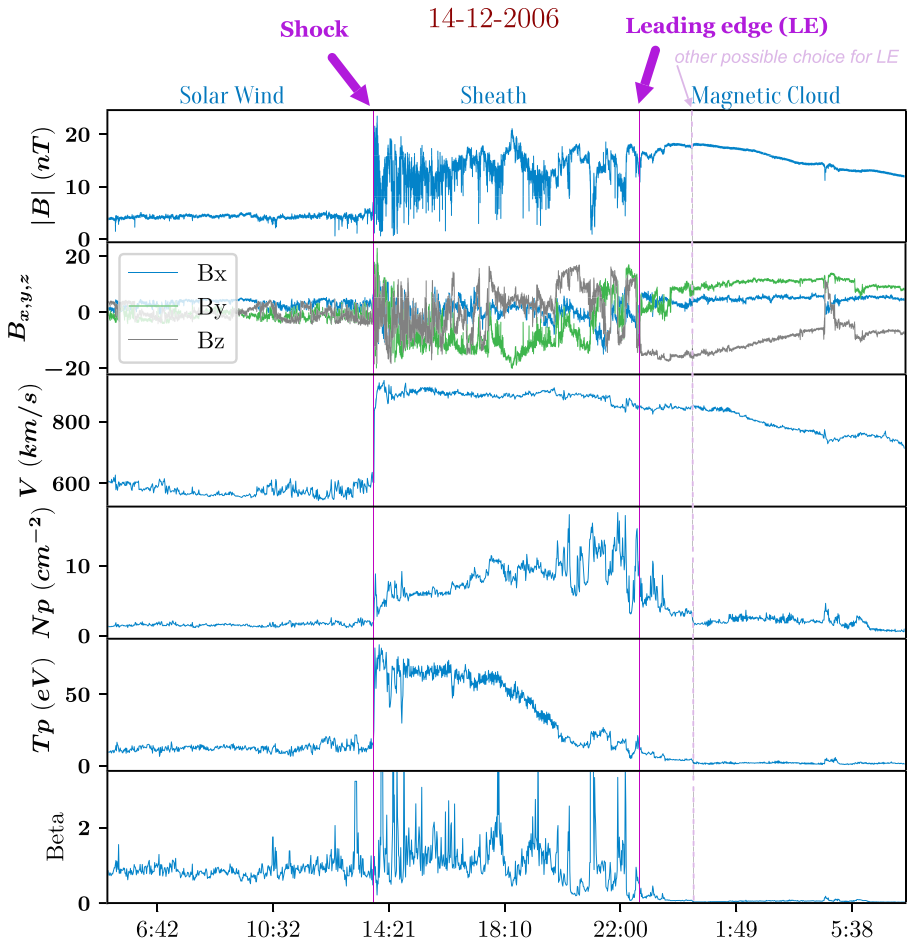

Figure 1. Observation from ACE spacecraft of a typical magnetic cloud event, centered on the sheath. From top to bottom are $|B|$ the amplitude of the magnetic field, $B_{x,y,z}$ its components, V the bulk flow velocity, N_p the proton density, T_p the proton temperature, and the plasma Beta. On this plot, and for all subsequent analysis of this event: the solar wind region spans from 14 December 2006 5:04 UT to 14 December 2006 14:14 UT, the sheath region spans from 14 December 2006 14:14 UT to 22:52 UT and the magnetic cloud region spans from 14 December 2006 22:52 UT to 15 December 2006 7:25 UT. Vertical purple bars separate the three different regions of the event, from left to right: the solar wind, the sheath, and the magnetic cloud. The dashed vertical bar shows another possible choice for the leading edge.

In the present paper we aim at characterizing the turbulence in the sheaths of magnetic clouds by considering the following questions:

– How does the spectral content of sheaths differ from the ones of the solar wind and magnetic clouds?
– What are the main parameters influencing the fluctuations in sheaths?

The following paper is organized as follows: In section 2, we present the list of events used as well as the means to retrieve the corresponding data. In section 3, we present a method to characterize the turbulence in sheaths, before showing in section 4 how the fluctuations in sheaths differ from those in their surrounding media. Section 5 draws a picture of what the fluctuations depend on and we conclude with section 6.

2. Data Description

In order to avoid mistaking phenomena arising from the sheaths themselves for phenomena arising from its interaction with another preceding event, it is important to study well-identified and isolated (far from any other event) magnetic cloud-driven sheaths. Masías-Meza et al. (2016) built a list containing 44 such events that we used for the present study. We used the data from the ACE spacecraft and in particular from the Magnetic Field Experiment with a 1-s resolution measurement of the magnetic field components and

from the Solar Wind Electron Proton Alpha Monitor (SWEPAM), with a 64-s resolution measurement of the velocity, density, and temperature (Stone et al., 1998). Both can be downloaded from the website (https://cdaweb.sci.gsfc.nasa.gov/index.html/). Two of the events ("18 March 2002" and "23 March 2002") from Table A.1 of Masías-Meza et al. (2016) do not have available data at 1-s resolution and have therefore been excluded from the present study.

Figure 1 shows an example of a typical event in the list. After a period of quiet solar wind the satellite encounters a shock, which marks the beginning of a highly turbulent sheath with high magnetic field amplitude, high velocity, high density, and high temperature. The time of the shock is easily identifiable by the simultaneous jumps of several quantities: We used the date and time given by the IPshock Database (http://ipshocks.fi/) when the shock is referenced there, and we defined it manually when not. The sheath itself is followed by a smoothly rotating magnetic field at a low plasma beta: the magnetic cloud. The transition between the sheath and magnetic cloud is called the leading edge of the magnetic cloud. The time of the leading edge of the magnetic cloud is somewhat more difficult to define, possibly controversial. It depends on criteria such as drop of the ratio of the plasma pressure to the magnetic pressure β, drop of the proton temperature T_p, beginning of a smooth rotation of the magnetic field B, and drop of the proton density N_p. Ambiguities arise when some of these criteria are not satisfied at the same moment. In these cases, we decided on a time and date for the leading edge ourselves. Because, as illustrated in Figure 1, the area surrounding the leading edge is not always clearly belonging to either the sheath or the magnetic cloud, we excluded ambiguous areas and focused only on zones unambiguously belonging to one or the other.

This led, for every event, to the definition of three *regions*: solar wind (SW), sheath (Sh) between the two solid lines, and magnetic cloud (MC) after the dashed line as illustrated in Figure 1.

As can be seen in Figure 1, we arbitrarily decided to analyze the data on a duration that depends on the length of the sheath: If T_{Sh} is the duration of the sheath, we analyzed the data for a total time of $3 \times T_{\mathrm{Sh}}$, with the solar wind in the first third, the sheath being placed in the middle, and the magnetic cloud in the last third. The same choice was made for every event.

3. Method: Analysis of a Single Event

3.1. Definition of the Fluctuations

We defined the fluctuations of the magnetic field as the variation around quantities averaged with the help of a sliding window (similarly to Tao et al., 2015) of $T_W = 15$-min length. The duration of the window has been chosen to follow the slower variations of the magnetic field while not filtering the faster ones:

$$\begin{aligned} \langle B_{x,y,z}\rangle(t) &= \frac{1}{T_W}\int_{t-T_W/2}^{t+T_W/2} B_{x,y,z}(\tau)\mathrm{d}\tau \\ \delta B_{x,y,z}(t) &= B_{x,y,z}(t) - \langle B_{x,y,z}\rangle(t) \end{aligned} \tag{1}$$

A good indicator of the nature of the fluctuations is the difference of behavior between fluctuations of the component of B, which is aligned with the average magnetic field $B_0 =< B >$, hereafter $\delta B_{||}$, and the fluctuations of the components that are perpendicular to B_0, hereafter $\delta B_{\perp}$.

In order to define those two quantities, we produced a moving orthonormal frame as described in equation 2:

$$\begin{aligned} \boldsymbol{b}_0 &= \frac{\boldsymbol{B}_0}{|\boldsymbol{B}_0|} \\ \boldsymbol{b}_1 &= \frac{\boldsymbol{e}_j \times \boldsymbol{B}_0}{|\boldsymbol{e}_j \times \boldsymbol{B}_0|} \\ \boldsymbol{b}_2 &= \frac{\boldsymbol{B}_0 \times (\boldsymbol{e}_j \times \boldsymbol{B}_0)}{|\boldsymbol{B}_0 \times (\boldsymbol{e}_j \times \boldsymbol{B}_0)|} \end{aligned} \tag{2}$$

In equation (2), for every region, e_j is automatically chosen from $[e_x, e_y, e_z]$ to maximize the quantity $\|e_j \times B_0\|$. Indeed, if the angle between e_j and B_0 is too small, the definition of the frame may be prone to error or high variability from a time step to the next (Duff et al., 2017). e_j itself is not perpendicular to B_0.

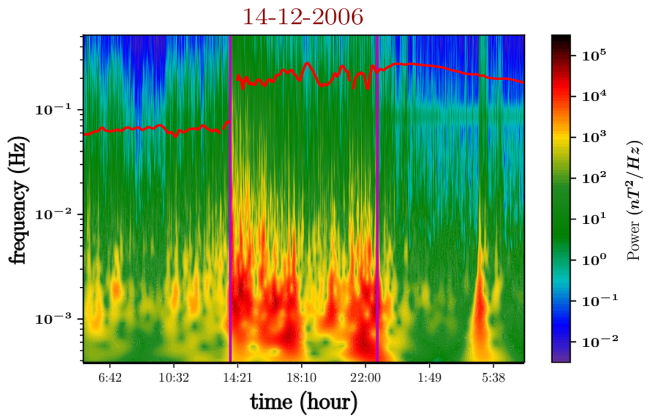

Figure 2. Morlet wavelets of the 14 December 2006 event. The vertical axis represents the frequency of waves. The horizontal axis represents the time. The color palette represents the amount of energy per unit volume and per unit frequency of the magnetic field: blue and green represent "low" energy content, while yellow and shades of red represent "high" energy content. Toward the top of the figure, the red line represents the gyrofrequency of protons $f_c = \omega_c/2\pi$ based on the value of B_0.

This comoving frame allowed us to define the parallel and perpendicular fluctuations by simple projections of δB on its axes:

$$\begin{aligned} \delta B_{||} &= (\boldsymbol{B} - \boldsymbol{B}_0) \cdot \boldsymbol{b}_0 \\ \delta B_{\perp 1} &= (\boldsymbol{B} - \boldsymbol{B}_0) \cdot \boldsymbol{b}_1 \\ \delta B_{\perp 2} &= (\boldsymbol{B} - \boldsymbol{B}_0) \cdot \boldsymbol{b}_2 \end{aligned} \tag{3}$$

3.2. Spectra

We applied the previous steps to the "14 December 2006" event shown in Figure 1 and used it to define the tools used in our statistical study.

Following the idea presented in de Wit et al. (2013), we used a Morlet wavelet transform (Torrence & Compo, 1998) to produce the spectra of $\delta B_{||}$, $\delta B_{\perp 1}$, and $\delta B_{\perp 2}$, respectively noted $\mathcal{W}(\delta B_{||})$, $\mathcal{W}(\delta B_{\perp 1})$ and $\mathcal{W}(\delta B_{\perp 2})$. We then defined $\mathcal{W}_{||} = \mathcal{W}(\delta B_{||})$, and $\mathcal{W}_{\perp} = \mathcal{W}(\delta B_{\perp 1}) + \mathcal{W}(\delta B_{\perp 2})$ as well as $\mathcal{W} = \mathcal{W}_{||} + \mathcal{W}_{\perp}$, which represents the total energy per unit volume and unit frequency of the fluctuations of B.

Figure 2 represents the temporal evolution of $\mathcal{W}(f, t)$ for the same event as in Figure 1 ("14 December 2006"): The horizontal axis represents the time, the vertical axis represents the frequency, and the colors represent the intensity $\mathcal{W}$ of the fluctuations, ($J{\cdot}m^{-3}\cdot Hz^{-1}$). We can see that the sheath region corresponds with a rise of $\mathcal{W}$. The green horizontal bar near 10^{-1} Hz is due to the satellite spin (Stone et al., 1998). As we averaged out the low frequencies through equation (1), we can see that the fluctuation spectra contains low power under 10^{-3} Hz. Then, there are two natural limits for the frequencies:

- A maximal limit to exclude the spin of the satellite $f_{\max} = 5 \cdot 10^{-2}$ Hz $< f_{\text{spin}}$.
- And a lower limit which comes from the definition of the mean field B_0: $f_{\min} = 2/(15\text{min.}) = 3 \cdot 10^{-3}$ Hz $> 2/T_W$. The factor 2 here was arbitrarily chosen to keep the analysis away from mathematical artifacts due to the edges of the sliding window, which arise below and around $1/T_W$.

Outside of these limits, the spectrum was not considered. Those limits also correspond to what is usually called the ULF bandwidth, which is relevant to interplanetary shocks (Kajdič et al., 2012), to the study of sheaths (Kilpua et al., 2013), and to the interaction of the solar wind with the terrestrial magnetosphere (Alimaganbetov & Streltsov, 2018; Kepko et al., 2002; Osmane et al., 2015). One can also see, at the shock, approximately at 14:21, that every frequency presents a heightened $\mathcal{W}$. The same thing can be seen around 5:38 when a small structure is encountered in the magnetic cloud. One problem with our definition of fluctuations (equation (1)) is that it does not apply well to jumps, such as shocks, large discontinuities, or small-scale structures. The Morlet transform is also particularly susceptible to these sudden changes and they should therefore be avoided in the analysis.

Figure 3 represents the power spectrum density ($\mathcal{PSD}$) of the magnetic fluctuations and their components, by integration on time of $\mathcal{W}(f, t)$ over time in each different region (solar wind, sheath, magnetic cloud), excluding the immediate surroundings of the shock and the leading edge. The power spectrum density of the parallel fluctuations $\mathcal{PSD}_{||}$ is represented in green, of the perpendicular fluctuations $\mathcal{PSD}_{\perp}$ in gray and the total in blue.

$$\mathcal{PSD}_{\perp,||}(f) = \frac{1}{T_{\text{region}}} \int_{T_{\text{region}}} \mathcal{W}_{\perp,||}(t, f)\mathrm{d}t \tag{4}$$

In Figure 3, we can see two clear trends. First, the fluctuation spectrum has much more power in the sheath than in the other regions investigated. We also note that the fluctuations in the solar wind preceding the sheath and in the following magnetic cloud have, on average, a similar power. And second, the gap between the green and the gray dotted lines is smaller in the middle panel than in the first one, which suggests more isotropic (or compressible) fluctuations in the sheath. On the other hand, the gap is very large in the right panel, the parallel power being so low that the total power is almost equal to the perpendicular power: The fluctuations in the magnetic cloud are very anisotropic (or almost incompressible).

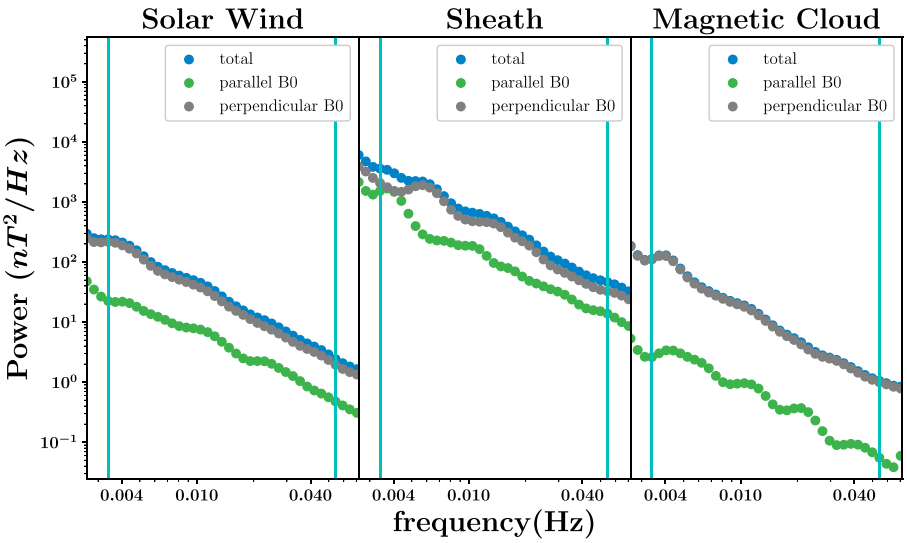

Figure 3. Spectrum of the fluctuations of the magnetic field (or power spectrum density) on each region of the 14 December 2006 event. The vertical axis represents the energy per unit volume and per unit frequency, and the horizontal axis represents the frequency. In blue is the total energy $\mathcal{PSD}$, in gray the energy of the fluctuations perpendicular to the mean magnetic field $\mathcal{PSD}_{\perp}$, and in green is the energy of the fluctuations parallel to the mean magnetic field $\mathcal{PSD}_{||}$. The cyan vertical bars mark the frequency limits inside of which the analysis was performed. A blue dashed line represents a linear fit of the spectrum between the frequency limits; the corresponding slope is reported in the upper-right corner.

3.3. Definition of Relevant Zones

As seen in the previous section 3.2, the Morlet transform, along with our definition of the fluctuations, does not apply well to jumps. The first consequence is that we did not analyze the data directly close to the shock or the leading edge of the magnetic cloud. Sheaths are made of a mixture of waves and small-scale structures, which occasionally form strong jumps. The second consequence, therefore, is that the best we could do was to avoid any visible and rapid jumps. For example, we show in Figure 4a possible selection of zones avoiding such jumps in the sheath of the "14 December 2006" event. The first zone, in red, starts slightly away from the shock and stops just before a rapid drop of B_z. The second zone, in pale blue, starts after this drop and stops before a large rise of both B_y and B_z. The third zone, in yellow, stops just before a small area where the amplitude of the mean magnetic field $|B_0|$ (in orange) does not follow the rapidly varying magnetic field $|B|$ (in blue). Lastly, the fourth zone, in blue, stops before a series of large variations of all the components of B. This choice allowed for a better analysis of the fluctuations without the inclusion of drastic changes.

Also, another type of problem is that some events include some unusual features: For example, there can be more organized structures within the sheath, some of them resembling flux ropes. The source for this is currently not understood. Likewise, short, highly turbulent zones can sometimes be found in a magnetic cloud, or a small area in the solar wind may occasionally be heavily perturbed by the shock. The definition of zones allowed us to exclude such unusual features from our analysis. No solution has been found yet to automate this choice of zones, which had to be made manually for every region of every considered event.

It is also possible to perform the analysis without introducing zones and therefore including every discontinuities and unusual features in the calculations. Tests show that this does not affect the general trends for the power and anisotropy but that the selection of zones enables a better separation of the different regions, which in turn improves their characterization. For example, without the selection of zones, the analysis of a magnetic cloud containing a short but strong discontinuity would yield values intermediate between a magnetic cloud and a sheath, and the same goes for a sheath including a small flux rope.

3.4. Definition of the Power and the Anisotropy of the Fluctuations

We used the wavelets analysis described in the section 3.2 on every zone, and, from it, we computed two quantities: The power P_{zone} and the anisotropy A_{zone}. The power P_{zone} represents the average quantity of

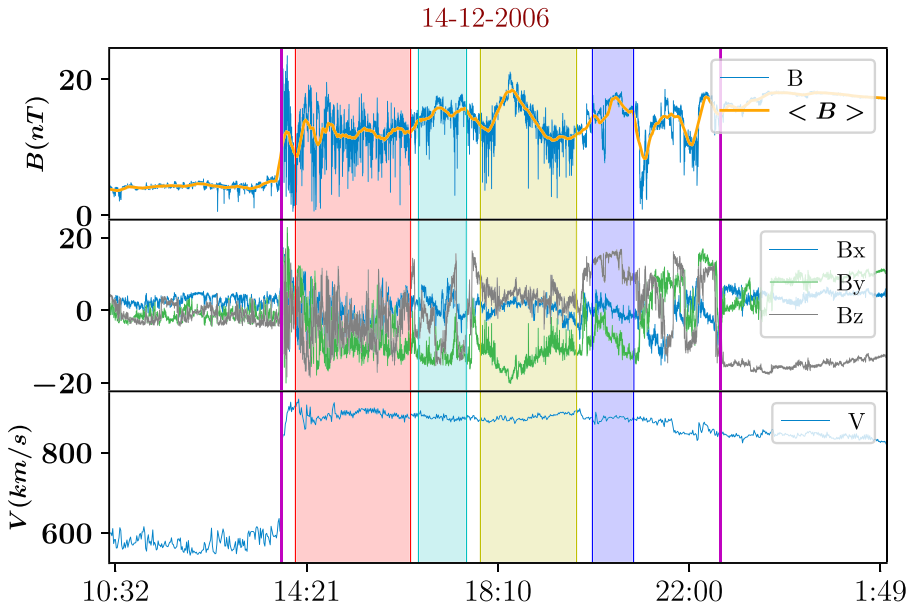

Figure 4. Here is a zoom on the sheath of the 14 December 2006 event, the sheath is delimited by the two purple vertical bars. Four different zones (in red, blue, yellow, and purple) were chosen manually to avoid jumps in the data.

energy per unit volume found in a zone between frequencies f_{min} and f_{max} and is defined as follows:

$$P_{\text{zone}\quad(\perp,||)} = \frac{1}{T_{\text{zone}}} \int_{T_{\text{zone}}} \int_{f_{\text{min}}}^{f_{\text{max}}} \mathcal{W}_{(\perp,||)}(t,f)\mathrm{d}f\,\mathrm{d}t \tag{5}$$

The anisotropy A measures the amount by which the measurements differ from the isotropic case:

$$A_{\text{zone}} = \frac{P_{\text{zone}\perp}}{2 \cdot P_{\text{zone}||}} \tag{6}$$

The factor 2 at the denominator allows $A = 1$ to represent the isotropic case, and $A > 1$ to represent stronger perpendicular fluctuations than parallel fluctuations.

Each region contains a few zones, and each of these are henceforth characterized by two scalar quantities: P_{zone} and A_{zone}. For each region we defined P_{region} and A_{region} as an average on the zones in that region:

$$\begin{aligned} P_{\text{region}} &= \frac{\sum_{[\text{zone}\in\text{region}]}(T_{\text{zone}} \cdot P_{\text{zone}})}{\sum_{[\text{zone}\in\text{region}]} T_{\text{zone}}} \\ A_{\text{region}} &= \frac{\sum_{[\text{zone}\in\text{region}]}(T_{\text{zone}} \cdot A_{\text{zone}})}{\sum_{[\text{zone}\in\text{region}]} T_{\text{zone}}} \end{aligned} \tag{7}$$

These quantities, defined for each region, are noted accordingly (P_{SW}, P_{Sh}, P_{MC}, A_{SW}, A_{Sh}, and A_{MC}). The results of this analysis for the "14 December 2006" event are given in Table 1.

Table 1 is a concise and more quantitative way of representing the already mentioned properties of the fluctuations in the "14 December 2006" event: Compared to the solar wind, there is an augmentation of the

Table 1
Power and Anisotropy of the Different Regions of the "14 December 2006" Event

P_{SW}	P_{Sh}	P_{MC}	
0.7	1.1	0.1	(nT^2)
A_{SW}	A_{Sh}	A_{MC}	
5.1	1.5	85.3	

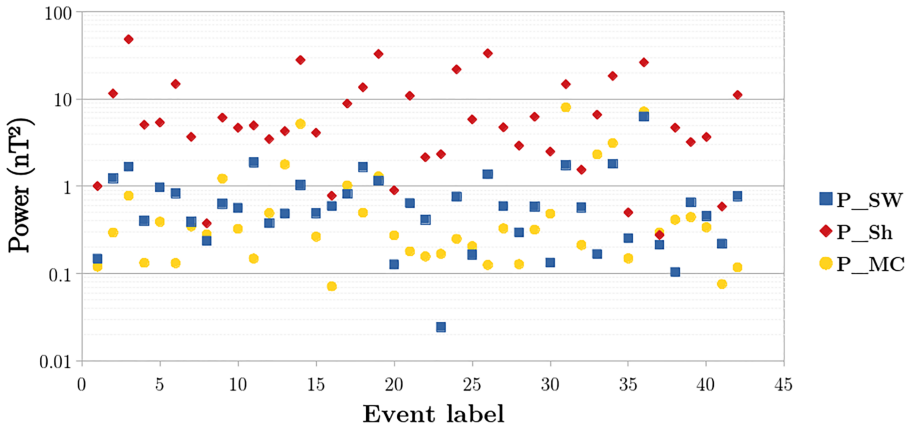

Figure 5. Every event is labeled by a number from 1 to 42 represented on the horizontal axis. The vertical axis is the value of the power P, which is the average quantity of energy per unit volume for a region of the event. The values of P vary between 0.01 and 100 nT^2. The power of the fluctuations P_{SW} in the solar wind preceding the sheath is represented in blue, P_{Sh} in the sheath in red, and P_{MC} in the magnetic cloud in yellow.

power in the sheath ($P_{SW} < P_{Sh}$) as well as a decrease of the anisotropy ($A_{SW} > A_{Sh}$). The fluctuations have a totally opposite behavior in the magnetic cloud, where their power drops ($P_{MC} < P_{Sh}$), and their anisotropy increases dramatically ($A_{MC} \gg A_{Sh}, A_{SW}$).

4. Power and Anisotropy in the 42 Events of Masías-Meza Et Al. (2016)

4.1. Power

Figure 5 presents, on the vertical axis, the values of P_{SW} (blue squares), P_{Sh} (red diamonds), and P_{MC} (yellow dots) for every event, labeled from 1 to 42 on the horizontal axis. We can observe that the values for the magnetic clouds (P_{MC}) and the solar wind (P_{SW}) are spread over approximately 1 order of magnitude, while they approximately span 2 orders of magnitude in the sheaths (P_{Sh}). We see a clear trend that the power of the fluctuations in the sheaths is higher by approximately an order of magnitude than in the other parts of the events. The average and standard deviation of the results are provided in Table 2.

In Table 2 we see that the distributions are quite spread, but there is a very clear trend that the sheaths contain about an order of magnitude more power in their fluctuations than the other regions. Solar wind and magnetic clouds seem to contain a similar range of power, which may seem quite surprising. We have no clear explanation but one possibility could be the following: when looking at Figure 1, we see indeed less fluctuations in the magnetic cloud compared with the solar wind, but this is mostly due to the high value of the mean magnetic field in the cloud, which may let us think that the fluctuations are smaller, by visual comparison. Also, it is quite common to plot or talk about the relative strength of fluctuations dB/B_0, which is indeed lower in magnetic clouds.

4.2. Anisotropy

Figure 6 presents, on the vertical axis, the values of A_{SW} (blue squares), A_{Sh} (red diamonds), and A_{MC} (yellow dots) for every event, labeled from 1 to 42 on the horizontal axis. Values of the anisotropy, range from 1 (*isotropic case*) to almost 91 (*very anisotropic case*). The values for each region (solar wind, sheath, or magnetic cloud) roughly spread over an order of magnitude. We can see that the sheaths tend to have a lower anisotropy (red diamonds), ranging from ~1 to 13, than the solar wind preceding them (blue squares), ranging from ~4 to 20. The magnetic clouds (yellow dots) tend to have a much higher anisotropy, with A_{MC} starting from 8 and reaching up to 91. Interestingly, some of the intervals of the solar wind (cyan stars) with higher values of A actually contain, upon close inspection, flux ropes. Most of these flux ropes are quite

Table 2
Average Power of the Magnetic Field Fluctuations and Its Standard Deviation in the Different Parts of the 42 Events in Square Nanoteslas

P_{SW}	P_{Sh}	P_{MC}	Unit
0.8 ± 1.0	9.3 ± 10.8	1.0 ± 1.8	(nT^2)

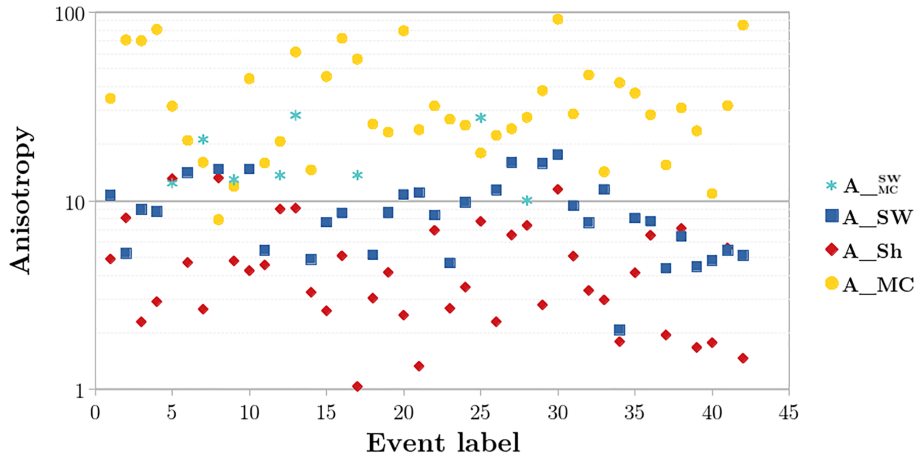

Figure 6. Every event is labeled by a number from 1 to 42 represented on the horizontal axis. The vertical axis is the value of A, the anisotropy of the fluctuations of the magnetic field. In blue we represent A in the solar wind preceding the sheath, in red we represent the value of A in the sheath, and in yellow we represent A in the magnetic cloud. In light blue, we represented the cases where the solar wind preceding the sheath was, in fact, a flux rope.

small and were understandably not identified as magnetic clouds, and one of them was an actual magnetic cloud (Case 30, in Masías-Meza et al.'s, 2016, list).

The results are summarized in Table 3, which shows that despite quite spread distributions, there is a very clear trend that the fluctuations in the sheath are much more isotropic than in the solar wind, whereas the fluctuations in the magnetic cloud are much more anisotropic than in any other region. We also provide the values of the compressibility, defined as the ratio of the power of the parallel fluctuations over the total power $C = \frac{P_{||}}{P}$, and computed using the same method as the power and anisotropy. The compressibility is a commonly used quantity that represents the same physics as the anisotropy. Indeed, because almost all the power of the fluctuations is contained in the perpendicular fluctuations, the compressibility and anisotropy have almost inverse behaviors. Therefore, the last results show that the plasma in sheaths is much more compressible than in the preceding solar wind and even more so than in the following magnetic cloud.

Our results for the solar wind and magnetic clouds match those of Leamon et al. (1998), who studied the power and the anisotropy of the fluctuations of a single event, but differ for the sheath. The differences noted for the sheath are easy to understand: First, Leamon et al. (1998) studied a single event, which may well have been a sheath with a relatively high anisotropy but still contained within the standard deviation given in Table 3. Second, they were not particularly interested in the sheath and used only a few fixed 1-hr-long windows to describe it: As seen in section 3.3 of the present paper, this is likely to be insufficient to study the highly complex fluctuations of the sheath. Another paper (Hu et al., 2013) reported variations from upstream to downstream of interplanetary shocks that are very similar to ours: Lower anisotropy and increased fluctuation power after the shock were found.

5. Correlations Between Sheaths' Fluctuations and Events' Main Parameters

So far in this paper, we chose two main parameters to characterize the fluctuations: the anisotropy and power, A and P. In Figure 7, every event is represented by a red dot in the (A_{Sh}, P_{Sh}) plane. We can see that

Table 3
Anisotropy and Compressibility: Average Value and Standard Deviation in the Different Parts of the Events

A_{SW}	A_{Sh}	A_{MC}
10 ± 6	5 ± 3	36 ± 23
C_{SW}	C_{Sh}	C_{MC}
0.07 ± 0.04	0.15 ± 0.08	0.02 ± 0.01

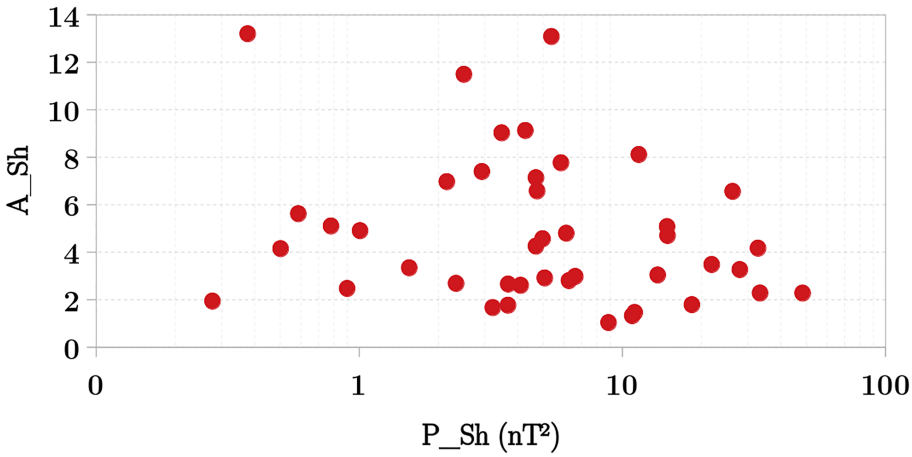

Figure 7. For every event, a red dot is placed on the diagram shown above with, on the vertical axis the anisotropy in the sheath and on the horizontal axis the power in the sheath.

the cloud of red dots is not forming any clear pattern: The values of A_{Sh} vary apparently randomly between 1 and 13 regardless of the value of P_{Sh}. In other words, the anisotropy does not depend on the power and therefore is not caused by a strong P. This test is important because it proves the nonredundancy of the chosen parameters P and A to characterize the fluctuations.

In the previous section, we have evidenced two main characteristics of the fluctuations in sheaths: high power P_{Sh} and low anisotropy A_{Sh}. We now analyze the dependency of the sheath's fluctuations (as represented by their power P_{Sh} and anisotropy A_{Sh}) on the surrounding media. Proxies for the surrounding media of the sheaths are (see definitions in Appendix A):

- parameters characterizing the solar wind: plasma density N_{SW}, magnetic field magnitude B_{SW}, ion velocity V_{SW}, Mach number in the solar wind M_A^{SW}, dynamic pressure in the solar wind P_{dyn}^{SW}, state of the fluctuations described by $\{P_{SW}, A_{SW}\}$
- parameters characterizing the shock: Mach number M_A, the ratio of thermal and magnetic pressure in the solar wind β_{up}, and the angle between the magnetic field in the solar wind and the shock's normal θ_{Bn}
- parameters characterizing the magnetic cloud: N_{MC}, B_{MC}, V_{MC}, M_A^{MC}, P_{dyn}^{MC}, $\{P_{MC}, A_{MC}\}$

Note that P_{SW}, A_{SW}, P_{MC}, and A_{MC} were computed on the solar wind and magnetic cloud regions, while all the other "SW" and "MC" parameters were computed on the "up" and "leading edge" interval as defined in Appendix A.

Among the different combinations that we tested, we show only the correlations which we deemed interesting. No clear conclusion could be extracted from the others.

In Figure 8 we compare the fluctuations in the sheaths with the fluctuations in the solar wind that precedes them, using A_{SW} and P_{SW} as proxies for the state of the fluctuations in the solar wind. We can see that the anisotropy in the sheath does not depend on the fluctuations already present in the solar wind: Indeed, in panels (a) and (c), we can see that both solar wind anisotropy and power can correspond to any value of the anisotropy in the sheath. This is also the case for the power in the sheath, which mostly does not seem to depend on A_{SW}. Indeed, panel (b) shows that high values of P_{Sh} are not reached when A_{SW} is high but only for a hardly significant number of cases, whereas values of P_{Sh} span the whole range when A_{SW} is low. The correlation between P_{Sh} and P_{SW}, in panel (d) is, on the other hand, stronger. Indeed, a linear fit roughly indicates a significant link between P_{Sh} and P_{SW}, while also making clear that P_{SW} is not the only factor at play (regression coefficient $R^2 = 0.42$). This may indicate that the power of the fluctuations in the solar wind has an effect on the fluctuations in the sheath. It is therefore suggested that highly turbulent sheaths are preceded by highly turbulent solar wind.

We now concentrate on the effect of the shock's parameters on the sheath's fluctuations. Indeed, the shock, by dissipating energy, is a priori the main reason for the existence of the turbulent sheath (Kataoka et al., 2005). We now analyze (Figure 9) the sheath anisotropy and power as a function of the shock's main

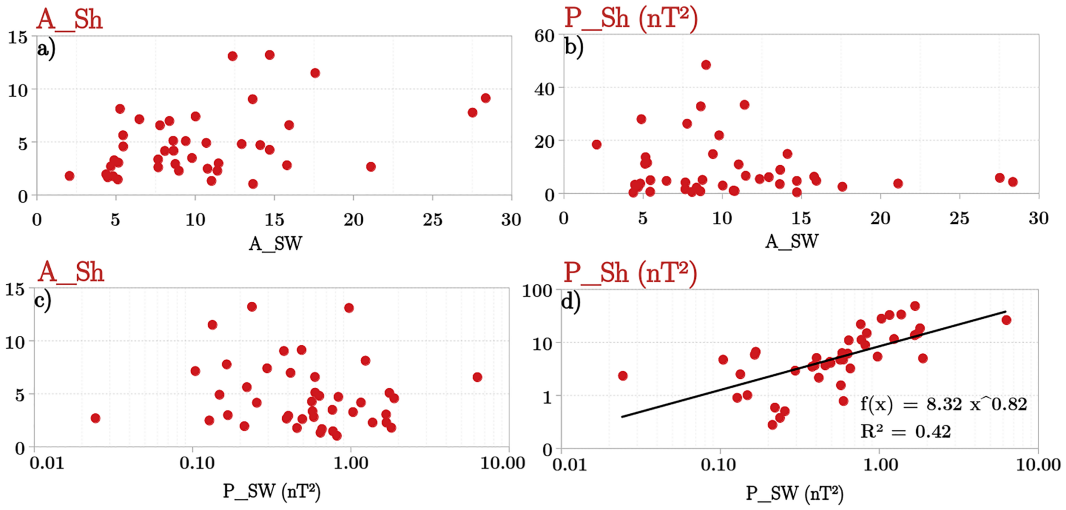

Figure 8. The four panels represent the state of the fluctuations in the sheath (P_{Sh}, A_{Sh}) versus the state the fluctuations in the solar wind (P_{SW}, A_{SW}) for every event. (a) A_{Sh} versus A_{SW}. (b) P_{Sh} versus A_{SW}. (c) A_{Sh} versus P_{SW}. (d) P_{Sh} versus P_{SW}, a linear regression is made (black line).

parameters M_A, β_{up}, and θ_{Bn} (see appendix for definitions). In Figure 9a we observe that for low values of the Alfvén Mach number ($M_A < 4$ or so) A_{Sh} can take on any value. The values of A_{Sh} seem to be more constrained at higher values of M_A. In panel (b), we see that for $M_A < 4$ or so, most P_{Sh} do not reach higher values that 10 nT^2. At higher values of M_A, the power tends to be high, which is expected due to the energy

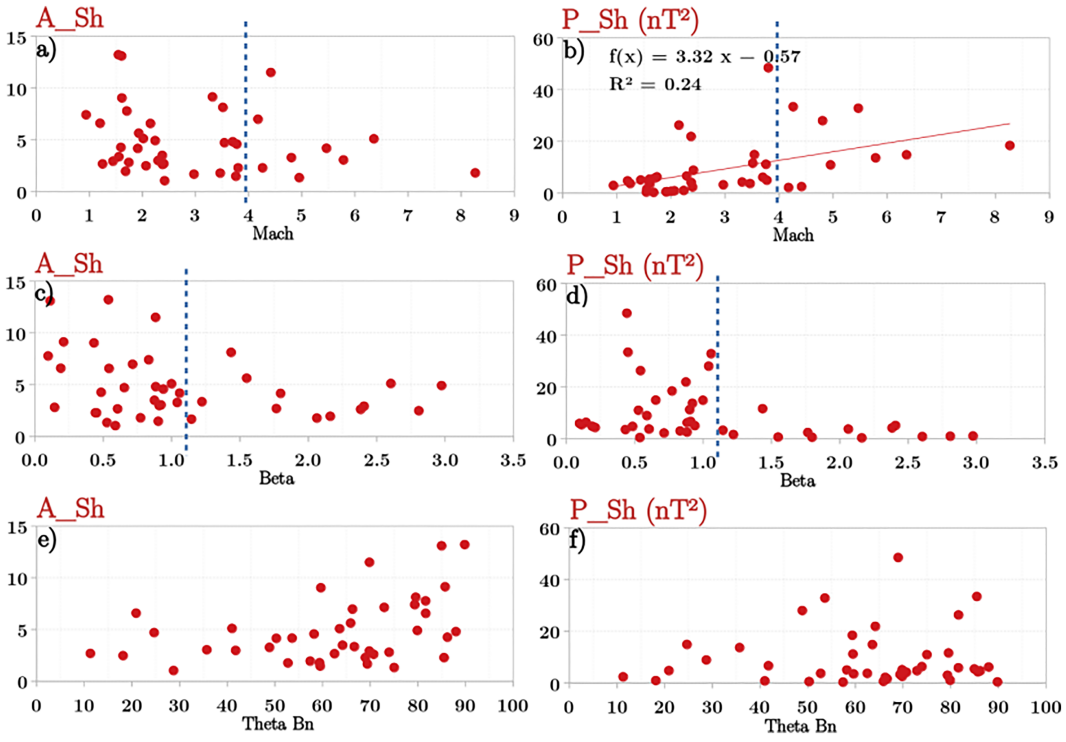

Figure 9. The two upper panels (a, b) represent the state of the fluctuations in the sheath against the shock's Mach number with a linear fit in panel (b), the two middle panels (c, d) represent the fluctuations in the sheath against the Beta upstream of the shock, and the two panels on the bottom (e, f) represent the fluctuations against the θ_{Bn}. Blue dashed vertical bars are visual aids showing a rough threshold of M_A and β.

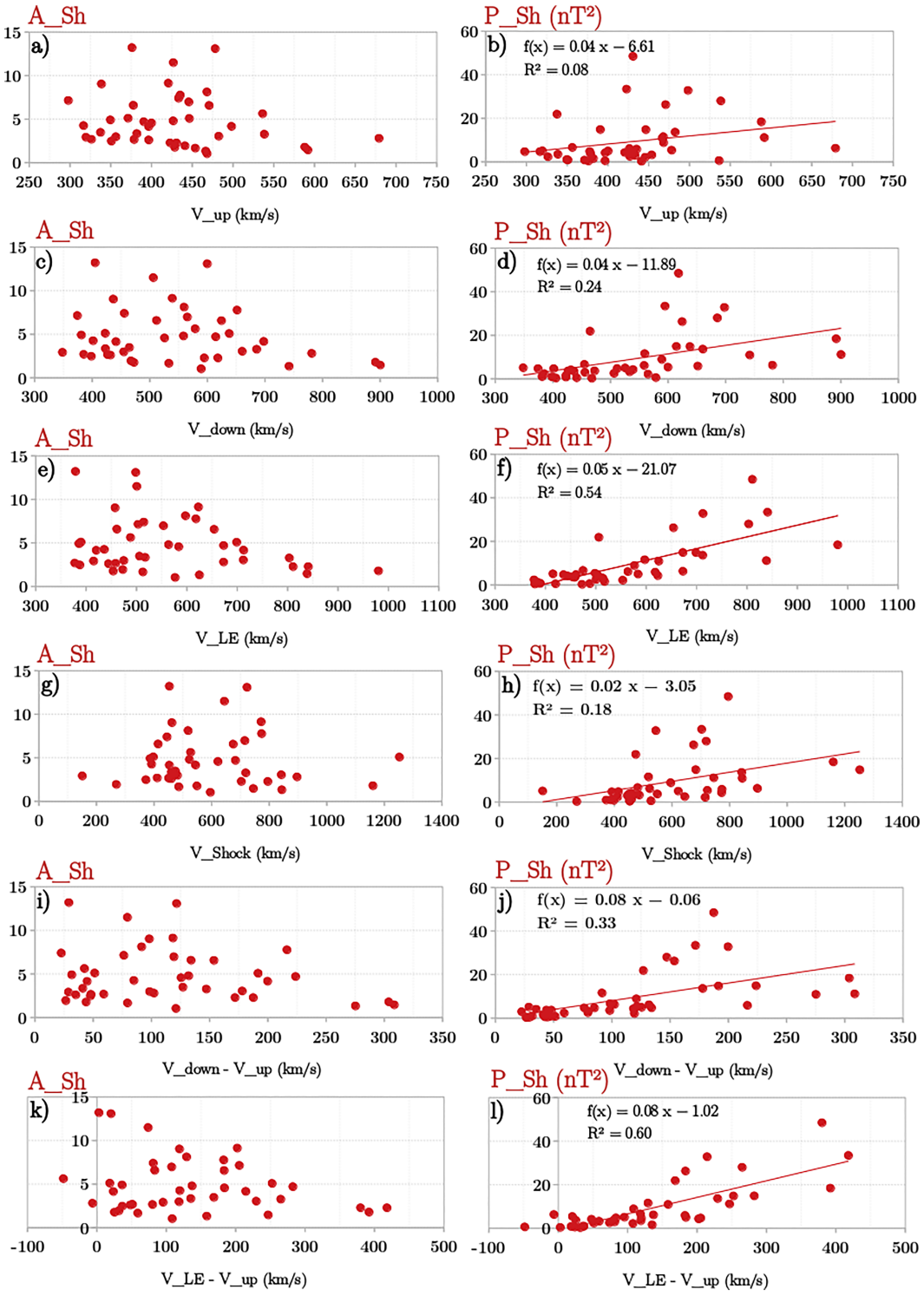

Figure 10. (a–l) The 12 panels represent the anistropy A_{Sh} and the power P_{Sh} of the fluctuations in the sheath plotted against different velocities. From top to bottom, those velocities are the velocity upstream of the shock, the velocity just downstream of the shock, the velocity of the leading edge of the magnetic cloud, the velocity of the shock, the difference between the velocities downstream and upstream of the shock, and the difference between the velocity of the leading edge and the velocity upstream of the shock.

dissipated by the shock, and the anisotropy tends to be low. We can see, though, that the regression coefficient of the linear fit in panel (b) is—maybe surprisingly—quite low, indicating that the shock's Mach number is not the main factor in producing the magnetic fluctuations in the sheath. Rather, it seems that the value $M_A \sim 4$ serves as a threshold for the state of the fluctuations downstream of the shock. Looking at panels (c) and (d), one can see that for $\beta_{up} > 1.1$ or so are associated with a smaller range of values for both A_{Sh} and P_{Sh}, whereas almost any type of fluctuations can be found at $\beta_{up} < 1.1$ or so. A possible interpretation is that high β_{up} events are plasmas dominated by the physics of thermal agitation, which is isotropic and potentially containing only weak magnetic fields, whereas low β_{up} events are dominated by the magnetic field, with potentially opposite consequences. Similarly, the range of values accessible to A_{Sh} and P_{Sh} seems to be constrained by θ_{Bn}. For $\theta_{Bn} < 45°$ (indicative of quasi-parallel shocks) there is a limited number of events but the trend shows that $A_{Sh} < 7$ and $P_{Sh} < 15\ nT^2$. Whereas for higher values of θ_{Bn} (indicative of quasi-perpendicular shocks), A_{Sh} and P_{Sh} explore the whole range of values. The fact that quasi-parallel shocks show a relatively low level of turbulence in the sheath is rather surprising (Treumann, 2009) but may be understood by a low compression by the shock of the magnetic field present in the solar wind due to the geometry.

We analyze in Figure 10 the dependency of the sheath fluctuations on different velocities relevant to the events' description (see the appendix). Indeed, the velocity of the event admits several definitions: the velocity of the solar wind upstream of the shock V_{up}, the velocity in the sheath downstream of the shock V_{down}, the velocity in the beginning of the magnetic cloud V_{LE}, and some combinations of the previous velocities: V_{shock}, $V_{down} - V_{up}$, $V_{LE} - V_{up}$. On all of the panels we can see a similar pattern: As the velocity increases, A_{Sh} can take on a smaller range of value, while P_{Sh} tends to increase. This pattern is similar to the one observed in Figure 9 with M_A, which is not surprising: The velocities can serve as a proxy for the energy to be dissipated by the shock. The only case where this trend is not observed is in panel g), where A_{Sh} seems to not be constrained by the value of V_{Shock}. It is quite clear on the two bottom panels (k) and (l) that $V_{LE} - V_{up}$ presents the best correlations with the anisotropy and power in the sheath. It is also worthy of note that the magnetic cloud's leading edge velocity V_{LE} (panels e and f) shows to be also quite a good predictor of the characteristics of the fluctuations.

6. Discussion and Conclusions

In this paper we focused on characterizing the magnetic fluctuations in magnetic clouds' sheaths, which are presently largely unknown. We started from a catalog of 44 isolated magnetic clouds, which are not disturbed by preceding and following events and identified by Masías-Meza et al. (2016). We mainly used 1-s magnetic field data from ACE near L1. We applied the Morlet wavelets transform on zones carefully defined in order to avoid jumps and unusual features in order to estimate the proper power spectral density of components parallel and perpendicular to the mean magnetic field. Two quantities were computed to characterize the fluctuations: The total power P and the anisotropy $A = \frac{P_\perp}{2P_{||}}$ (section 3). It was found that P reaches an average value of about $10\ nT^2$ in the sheaths, significantly exceeding, by a factor of about 10, the corresponding power in the preceding solar wind and the following magnetic cloud. Conversely, the anisotropy A takes its smallest values in sheaths, 5 on average and sometimes close to the isotropy level ($A = 1$), while it ranges around 10 in the preceding solar wind and reaches the largest values in magnetic clouds, 36 on average and sometimes almost 100 (section 4). In terms of the compressibility defined as $C = \frac{P_{||}}{P}$, the plasma in sheaths (~ 0.15 on average) is more compressible than in the preceding solar wind (~ 0.07) and much more than in almost incompressible magnetic clouds (~ 0.02). Section 5 reveals that there is no correlation between power and anisotropy in sheaths. Therefore, isotropy is not necessarily a consequence of powerful fluctuations. P and A can be regarded as independent quantities, which justifies the use of both to describe the characteristics of the fluctuations of sheaths.

We then estimated the role of the surrounding media on the characteristics of the fluctuations in sheaths. In line with Kilpua et al. (2013), our results show that one of the most significant parameters is the speed of the magnetic clouds: Larger powers are found in sheaths driven by faster magnetic clouds ($V_{LE} > 750$ km/s), their velocity V_{LE} being estimated at their leading edge. The anisotropy in sheaths also reacts to the cloud velocity: It can take any value within a wide range from 1 to 14 in sheaths related to slow clouds, but it is confined in the range 1–5, that is, closer to isotropy when the sheaths are associated with fast clouds.

Conversely, we found no correlation of sheath characteristics with the amplitude of the cloud magnetic field. Finally, we can give the following interpretation of the increased power: The enhanced kinetic energy carried by fast magnetic clouds is dissipated in the sheath, giving rise through turbulent processes to small-scale structures, such as these powerful magnetic fluctuations observed in the sheaths.

Another significant parameter for the sheath fluctuations is the turbulence of the pristine solar wind upstream the shock. The magnetic fluctuation power in the sheaths increases with that of the solar wind, with the most powerful sheaths (typically above 10 nT^2) observed after intervals of highly turbulent solar wind (typically above 1 nT^2). Conversely, the sheath anisotropy does not seem to be affected by the solar wind power or anisotropy. Also parameters such as the solar wind density or dynamic pressure do not seem to play a role for sheath fluctuations. Therefore, it seems that a high level of magnetic fluctuations preexisting in the solar wind likely represents a good seed for turbulence in the sheath downstream of the shock.

We estimated the influence of the parameter β computed in the solar wind just upstream of the shock. Below a threshold value of about 1.1, the fluctuation power and anisotropy in the sheath cover a wide range of values without any obvious correlation. Above this threshold value of 1.1, both the sheath power and anisotropy reduce to weak values. In this case, the thermal energy exceeds the magnetic energy and therefore the magnetic fluctuations might become a secondary effect, possibly less powerful and guided than in presence of a strong magnetic field.

We also analyzed the dependency of the sheath's characteristics on the parameters of the shock. We found that both sheath power and anisotropy correlate only poorly with the shock velocity unlike the cloud velocity. The shock Mach number appears to be a more relevant parameter separating the events in two groups apart a threshold value around 4. Below it, the fluctuation power is low and the anisotropy varies over a wide range, while above it, the sheath fluctuations become more powerful and isotropic. Indeed, the shock's Alfvén Mach number acts as a proxy for the energy dissipation at the shock and plays, in this regard, a similar role to the cloud velocity. The shock angle also seems to play a role. Downstream of a quasi-perpendicular shock ($\theta_{Bn} > 45°$), both the fluctuation power and anisotropy in the sheaths cover a wide range of values. Downstream of quasi-parallel shocks ($\theta_{Bn} < 45°$), there is a trend toward more isotropy, which is expected. However, the fluctuation power goes down to low values, which is the opposite of what we find behind the terrestrial bow shock (Blanco-Cano et al., 2006; Du et al., 2008; Narita et al., 2006). The low number of quasi-parallel shocks in our set of data does not allow us to make any conclusion. The latter effect (low power) might be linked to a weaker compression of the interplanetary magnetic field in quasi-parallel than in quasi-perpendicular configurations, leading to weaker magnetic fields in the sheath and maybe to weaker fluctuations. Such an effect would require to be more deeply investigated.

In summary, in clouds' sheaths, the magnetic fluctuations which are the most powerful and the closest to isotropy are likely to be driven by fast magnetic clouds with typical velocities larger than 750 km/s as estimated at their leading edge, interacting with an already turbulent solar wind with a magnetic fluctuation power typically larger than 1 nT^2, and with a high Alfvén Mach number at shock (typically above 4). The relations with the shock angle and β upstream are a little more complex. Downstream of quasi-perpendicular shocks and high-β solar wind, the observed sheaths show a trend toward isotropy but also a weak fluctuation power, while downstream of quasi-perpendicular shocks and low-β solar wind, both fluctuation power and anisotropy cover a wide range of values.

Interestingly, Leamon et al. (1998) studied an ICME encountering an undisturbed, slow solar wind. The magnetic cloud in that paper has quite a low speed and a high beta prior to the sheath. Therefore, the sheath in Leamon et al. (1998) has all the ingredients to present a high anisotropy, and a low power, which is what the authors found.

In the case of the solar wind, it has been shown that fluctuations with large-amplitude and low anisotropy imply a good coupling of the solar wind with the magnetosphere (Jankovičvá et al., 2008). Our results suggest that turbulent sheaths preceding magnetic cloud present a high energy content of their fluctuations, as well as a low anisotropy, which may favor their geoeffectiveness.

Future observational work will be needed in order to further investigate the evolution of fluctuations inside the sheaths themselves. Indeed, it will be interesting to compare the evolution of the fluctuations of the

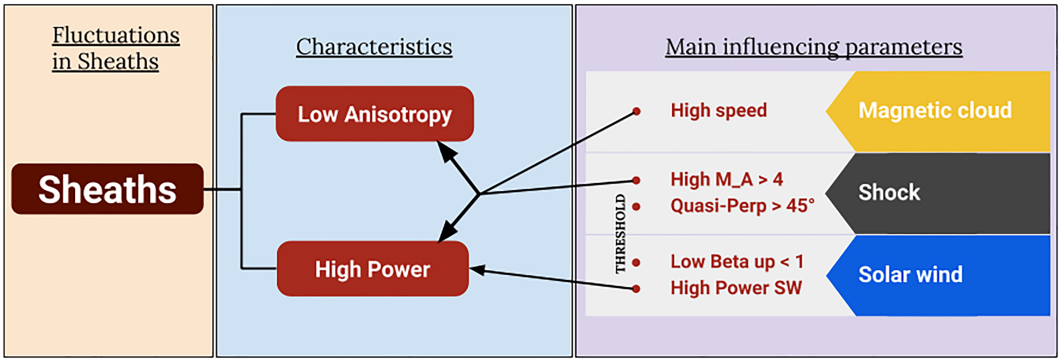

Figure 11. Characterizing the fluctuations in sheaths by two numbers (power and anisotropy), we find that, compared with the solar wind, sheaths have high power and low anisotropy. This is further enhanced when certain parameters are found in the magnetic cloud, shock and solar wind surrounding the sheaths.

magnetic field with other fluctuations such as the velocity or dynamic pressure fluctuations. It is also of importance for geoeffectiveness to estimate the fluctuation characteristics between the different sheath regions from the shock to the cloud's leading edge (as suggested by Kilpua et al., 2013).

7. Summary

From a list of 42 isolated events (Masías-Meza et al., 2016), we characterized the fluctuations in the three regions (solar wind, sheath, and magnetic cloud) based on their power and anistotropy, which appear as two independent parameters. Figure 11 gives a brief summary of the results.

- The fluctuations have much more power in the sheath (P_{Sh} ~9 nT^2) than in the preceding solar wind and following magnetic cloud ($P_{SW} \simeq P_{MC} \sim 0.9$ nT^2), by an order of magnitude.
- The fluctuations seem to be more isotropic (and thus more compressible) in the sheath ($A_{Sh} \sim 5$, or correspondingly $C_{Sh} \sim 0.15$) than in the solar wind ($A_{SW} \sim 10$, or $C_{SW} \sim 0.07$), and are much more anisotropic (and thus more incompressible) in the magnetic cloud ($A_{MC} \sim 36$, or $C_{MC} \sim 0.02$)

The parameters that have the strongest influence on the power and anisotropy of the fluctuations in the sheaths of these events, are mainly the following:

(i) the speed of the magnetic cloud,
(ii) the Alfvén Mach number of the shock, as those parameters increase, the power and isotropy of the fluctuations in the sheath increase.
(iii) the preexisting fluctuation power in the solar wind to which the power in the sheath is roughly proportional but not the anisotropy.
(iv) the angle between the shock's normal and the magnetic field upstream of the shock,
(v) the beta of the solar wind,

which have a somewhat more subtle role. $\beta \sim 1$ in the solar wind serves as a threshold above which both the power and the anisotropy of the fluctuations in sheaths drop significantly. Similarly, quasi-parallel shocks have both low power and anisotropy whereas any values of P_{Sh} and A_{Sh} can be found next to quasi-perpendicular shocks.

Appendix A: Definition of the Events' Main Parameters

We define in this sections the parameters against which the power and anisotropy of sheath are plotted in section 5. Some of these parameters depend on upstream and downstream (to the shock) values. We define the interval of time upstream as $\Delta t_{up} = [t_{shock} - 30\text{min}, t_{shock} - 15\text{min}]$ and the interval of time downstream as $\Delta t_{down} = [t_{shock} + 15\text{min}, t_{shock} + 30\text{min}]$. These intervals are defined as such in order to be the same length as the sliding window we use for all our averages and away from the transition layers by the same length. Any quantity Q computed on the interval Δt_{up} or Δt_{down} is respectively noted Q_{up} or Q_{down}.

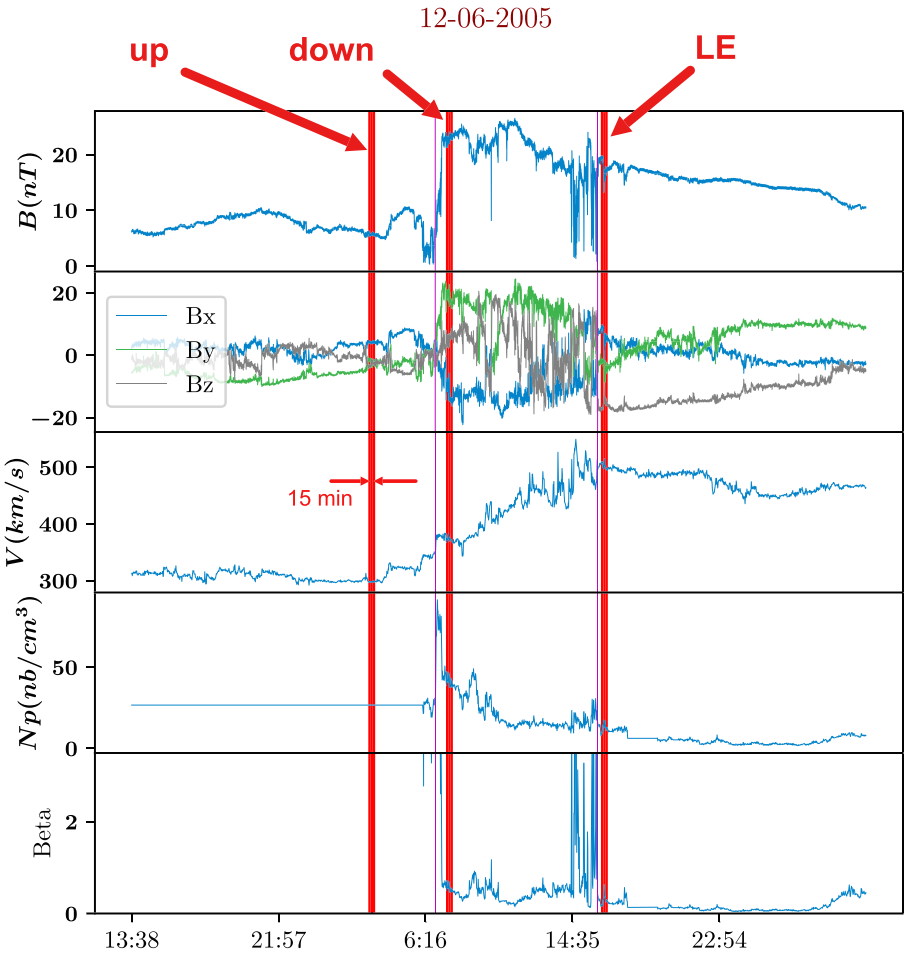

Figure A1. The three red vertical bands marked "up," "down," and "LE" represent the small areas of 15-min length used to compute most of the event's main parameters. For this particular event "upstream" is defined, manually, away from the shock to avoid a zone that is not representative of the pristine solar wind ahead of the event.

For a dozen of cases, taking data just upstream and downstream of the shock seemed flawed because of, for example, the presence of a structure just in front of the shock. In those cases, we defined manually upstream in the "pristine" solar wind. Any quantity used to describe the solar wind is then computed on the interval of time Δt_{up}.

Another area of interest is just after the leading edge of the magnetic cloud: $\Delta t_{\mathrm{LE}} = [t_{\text{leading edge}} + 15\text{min}, t_{\text{leading edge}} + 30\text{min}]$. Quantities representative of the magnetic clouds are computed in the interval of time Δt_{LE}. Any quantity Q computed on the interval Δt_{LE} is noted Q_{LE}.

Those areas are represented in Figure A1

Parameters describing the solar wind, defined on Δt_{up}.

$$
\begin{aligned}
N_{\mathrm{SW}} &= \langle N \rangle_{\mathrm{up}} \\
B_{\mathrm{SW}} &= \langle |\boldsymbol{B}| \rangle_{\mathrm{up}} \\
V_{\mathrm{SW}} &= V_{\mathrm{up}} = \langle |\boldsymbol{V}| \rangle_{\mathrm{up}} \\
V_A^{\mathrm{up}} &= \langle v_A \rangle_{\mathrm{up}} = \left\langle \frac{B}{\sqrt{\mu_0 N_p m_p}} \right\rangle_{\mathrm{up}} \\
M_A^{\mathrm{up}} &= \frac{V_{\mathrm{up}}}{V_A^{\mathrm{up}}}
\end{aligned}
\tag{A1}
$$

P_{SW} and A_{SW} are the ones defined in section 3.4

Parameters describing the magnetic cloud, defined on Δt_{LE}.

$$\begin{aligned} N_{\mathrm{MC}} &= \langle N \rangle_{\mathrm{LE}} \\ B_{\mathrm{MC}} &= \langle |\boldsymbol{B}| \rangle_{\mathrm{LE}} \\ V_{\mathrm{MC}} &= V_{\mathrm{LE}} = \langle |\boldsymbol{V}| \rangle_{\mathrm{LE}} \\ V_A^{\mathrm{LE}} &= \langle v_A \rangle_{\mathrm{LE}} = \left\langle \frac{B}{\sqrt{\mu_0 N_p m_p}} \right\rangle_{\mathrm{LE}} \\ M_A^{\mathrm{LE}} &= \frac{V_{\mathrm{LE}}}{V_A^{\mathrm{LE}}} \end{aligned} \tag{A2}$$

P_{MC} and A_{MC} are the ones defined in section 3.4.

Parameters describing the shock. We use the definitions given at https://ipshocks.fi/documentation to define the main shocks' parameters: Alfvén Mach (M_A), plasma beta upstream of the shock (β), the angle between the normal of the shock, and the magnetic field upstream of the shock (θ_{Bn}).

shock normal

$$\hat{\boldsymbol{n}} = \frac{(\boldsymbol{B}_{\mathrm{down}} - \boldsymbol{B}_{\mathrm{up}}) \times ((\boldsymbol{B}_{\mathrm{down}} - \boldsymbol{B}_{\mathrm{up}}) \times (\boldsymbol{V}_{\mathrm{down}} - \boldsymbol{V}_{\mathrm{up}}))}{|(\boldsymbol{B}_{\mathrm{down}} - \boldsymbol{B}_{\mathrm{up}}) \times ((\boldsymbol{B}_{\mathrm{down}} - \boldsymbol{B}_{\mathrm{up}}) \times (\boldsymbol{V}_{\mathrm{down}} - \boldsymbol{V}_{\mathrm{up}}))|} \tag{A3}$$

shock speed

$$V_{\mathrm{shock}} = \left| \frac{N_p^{\mathrm{down}} \boldsymbol{V}_{\mathrm{down}} - N_p^{\mathrm{up}} \boldsymbol{V}_{\mathrm{up}}}{N_p^{\mathrm{down}} - N_p^{\mathrm{up}}} \cdot \hat{\boldsymbol{n}} \right| \tag{A4}$$

Alfvén Mach number

$$M_A = \frac{|\boldsymbol{V}_{\mathrm{up}} \cdot \hat{\boldsymbol{n}} - V_{\mathrm{shock}}|}{V_A^{\mathrm{up}}} \tag{A5}$$

Upstream plasma beta

$$\beta^{\mathrm{up}} = \langle \beta \rangle_{\mathrm{up}} = \left\langle \frac{2\mu_0 k_B N_p (T_p + T_e)}{B^2} \right\rangle_{\mathrm{up}} \tag{A6}$$

shock theta

$$\theta_{Bn} = \frac{180°}{\pi} \arccos\left(\frac{|\boldsymbol{B}_{\mathrm{up}} \cdot \hat{\boldsymbol{n}}|}{|\boldsymbol{B}_{\mathrm{up}}| \quad |\hat{\boldsymbol{n}}|} \right) \tag{A7}$$

A few more definitions

Velocities

$$\begin{aligned} V_{\mathrm{down}} &= \langle |\boldsymbol{V}| \rangle_{\mathrm{down}} \\ V_{\mathrm{down}} - V_{\mathrm{up}} &= \langle |\boldsymbol{V}| \rangle_{\mathrm{down}} - \langle |\boldsymbol{V}| \rangle_{\mathrm{up}} \\ V_{\mathrm{LE}} - V_{\mathrm{up}} &= \langle |\boldsymbol{V}| \rangle_{\mathrm{LE}} - \langle |\boldsymbol{V}| \rangle_{\mathrm{up}} \end{aligned} \tag{A8}$$

Acknowledgments
We are thankful to Gautier Nguyen for a part of the code used to easily retrieve ACE data and to Roland Grappin for enlightening discussions. This work received financial support by the program "Investissements d avenir" under the Reference ANR-11-IDEX-0004-02 (Plas@Par). We are indebted to ANR for the project TEMPETE (ANR-17-CE31-0016). Numerical simulations which were useful to interpret the results described in this paper were performed on the supercomputer center "IDRIS" institute of the Centre National de la Recherche Scientifique (CNRS) (http://www.idris.fr). We are also thankful to the two anonymous reviewers of this article, who helped in making it better organized and easier to read. All relevant data can be accessed from the website (https://cdaweb.sci.gsfc.nasa.gov/index.html/).

References

Ala-Lahti, M. M., Kilpua, E. K. J., Dimmock, A. P., Osmane, A., Pulkkinen, T. I., & Soućek, J. (2018). Statistical analysis of mirror mode waves in sheath regions driven by interplanetary coronal mass ejection. *Annales Geophysicae*, *36*(3), 793–808. https://doi.org/10.5194/angeo-36-793-2018

Alimaganbetov, M., & Streltsov, A. V. (2018). ULF waves observed during substorms in the solar wind and on the ground. *Journal of Atmospheric and Solar-Terrestrial Physics*, *181*, 10–18. https://doi.org/10.1016/j.jastp.2018.10.007

Blanco-Cano, X., Omidi, N., & Russell, C. T. (2006). Macrostructure of collisionless bow shocks: 2. ULF waves in the foreshock and magnetosheath. *Journal of Geophysical Research*, *111*, A10205. https://doi.org/10.1029/2005JA011421

Borovsky, J. E. (2003). Role of solar wind turbulence in the coupling of the solar wind to the Earth's magnetosphere. *Journal of Geophysical Research*, *108*(A6), 1246. https://doi.org/10.1029/2002JA009601

Burlaga, L. F. E. (1991). Physics of the inner heliosphere II: Particles, waves and turbulence (pp. 1–22). https://doi.org/10.1007/978-3-642-75364-0_1

Chi, Y., Shen, C., Wang, Y., Xu, M., Ye, P., & Wang, S. (2016). Statistical study of the interplanetary coronal mass ejections from 1995 to 2015. *Solar Physics*, *291*(8), 2419–2439. https://doi.org/10.1007/s11207-016-0971-5

de Wit, T. D., Alexandrova, O., Furno, I., Sorriso-Valvo, L., & Zimbardo, G. (2013). Methods for characterising microphysical processes in plasmas. *Space Science Reviews*, *178*(2-4), 665–693. (arXiv: 1306.5303)https://doi.org/10.1007/s11214-013-9974-9

Du, J., Wang, C., Song, P., & Zhang, T. (2008). Low-frequency fluctuations in the magnetosheath: Double Star TC-1 and Cluster observations. *Science in China Series E Technological Sciences*, *51*(10), 1626–1638. https://doi.org/10.1007/s11431-008-0250-2

Duff, T., Burgess, J., Christensen, P., Hery, C., Kensler, A., Liani, M., & Villemin, R. (2017). Building an orthonormal basis, Revisited. *Journal of Computer Graphics Techniques*, *6*(1), 8.

Dungey, J. W. (1961). Interplanetary magnetic field and the auroral zones. *Physical Review Letters*, *6*(2), 47–48. https://doi.org/10.1103/PhysRevLett.6.47

Echer, E., Gonzalez, W. D., & Tsurutani, B. T. (2008). Interplanetary conditions leading to superintense geomagnetic storms (Dst $\leq$- 250 nT) during solar cycle 23. *Geophysical Research Letters*, *35*, L06S03. https://doi.org/10.1029/2007GL031755

Gonzalez, W. D., Echer, E., Clua-Gonzalez, A. L., & Tsurutani, B. T. (2007). Interplanetary origin of intense geomagnetic storms (Dst $<$ 100 nT) during solar cycle 23. *Geophysical Research Letters*, *34*, L06101. https://doi.org/10.1029/2006GL028879

Gonzalez, W. D., Joselyn, J. A., Kamide, Y., Kroehl, H. W., Rostoker, G., Tsurutani, B. T., & Vasyliunas, V. M. (1994). What is a geomagnetic storm? *Journal of Geophysical Research*, *99*(A4), 5771–5792. https://doi.org/10.1029/93JA02867

Gonzalez, W. D., & Tsurutani, B. T. (1987). Criteria of interplanetary parameters causing intense magnetic storms (Dst of less than −100 nT). *Planetary and Space Science*, *35*, 1101–1109. https://doi.org/10.1016/0032-0633(87)90015-8

Gonzalez, W. D., Tsurutani, B. T., Gonzalez, A. L. C., Smith, E. J., Tang, F., & Akasofu, S. I. (1989). Solar wind-magnetosphere coupling during intense magnetic storms (1978–1979). *Journal of Geophysical Research*, *94*(A7), 8835–8851. https://doi.org/10.1029/JA094iA07p08835

Guo, J., Feng, X., Emery, B. A., Zhang, J., Xiang, C., Shen, F., & Song, W. (2011). Energy transfer during intense geomagnetic storms driven by interplanetary coronal mass ejections and their sheath regions: Energy transfer. *Journal of Geophysical Research*, *116*, A05106. https://doi.org/10.1029/2011JA016490

Hu, Q., Zank, G. P., Li, G., & Ao, X. (2013). A power spectral analysis of turbulence associated with interplanetary shock waves. *Solar Wind 13*, *1539*, 175–178. https://doi.org/10.1063/1.4811016

Huttunen, K. E. J., & Koskinen, H. E. J. (2004). Importance of post-shock streams and sheath region as drivers of intense magnetospheric storms and high-latitude activity, *Annales Geophysicae* (Vol. 22, pp. 1729–1738). https://doi.org/10.5194/angeo-22-1729-2004

Huttunen, K. E. J., Schwenn, R., Bothmer, V., & Koskinen, H. E. J. (2005). Properties and geoeffectiveness of magnetic clouds in the rising, maximum and early declining phases of solar cycle 23, *Annales Geophysicae* (Vol. 23, pp. 625–641). https://doi.org/10.5194/angeo-23-625-2005

Jankovičvá, D., Vörös, Z., & Šimkanin, J. (2008). The effect of upstream turbulence and its anisotropy on the efficiency of solar wind-magnetosphere coupling. *Nonlinear Processes in Geophysics*, *15*(4), 523–529. https://doi.org/10.5194/npg-15-523-2008

Kajdič, P., Blanco-Cano, X., Aguilar-Rodriguez, E., Russell, C. T., Jian, L. K., & Luhmann, J. G. (2012). Waves upstream and downstream of interplanetary shocks driven by coronal mass ejections: Waves associated with IP shocks. *Journal of Geophysical Research*, *117*, A06103. https://doi.org/10.1029/2011JA017381

Kataoka, R., Watari, S., Shimada, N., Shimazu, H., & Marubashi, K. (2005). Downstream structures of interplanetary fast shocks associated with coronal mass ejections. *Geophysical Research Letters*, *32*, L12103. https://doi.org/10.1029/2005GL022777

Kepko, L., Spence, H. E., & Singer, H. J. (2002). ULF waves in the solar wind as direct drivers of magnetospheric pulsations. *Geophysical Research Letters*, *29*(8), 1197. https://doi.org/10.1029/2001GL014405

Kilpua, E. K. J., Balogh, A., von Steiger, R., & Liu, Y. D. (2017). Geoeffective properties of solar transients and stream interaction regions. *Space Science Reviews*, *212*(3-4), 1271–1314. https://doi.org/10.1007/s11214-017-0411-3

Kilpua, E. K. J., Hietala, H., Koskinen, H. E. J., Fontaine, D., & Turc, L. (2013). Magnetic field and dynamic pressure ULF fluctuations in coronal-mass-ejection-driven sheath regions. *Annales Geophysicae*, *31*(9), 1559–1567. https://doi.org/10.5194/angeo-31-1559-2013

Kilpua, E. K. J., Koskinen, H. E. J., & Pulkkinen, T. I. (2017). Coronal mass ejections and their sheath regions in interplanetary space. *Living Reviews in Solar Physics*, *14*, 5. https://doi.org/10.1007/s41116-017-0009-6

Kilpua, E. K. J., Li, Y., Luhmann, J. G., Jian, L. K., & Russell, C. T. (2012). On the relationship between magnetic cloud field polarity and geoeffectiveness. *Annales Geophysicae*, *30*(7), 1037–1050. https://doi.org/10.5194/angeo-30-1037-2012

Leamon, R. J., Smith, C. W., & Ness, N. F. (1998). Characteristics of magnetic fluctuations within coronal mass ejections: The January 1997 event. *Geophysical Research Letters*, *25*(14), 2505–2508. https://doi.org/10.1029/98GL00305

Masías-Meza, J. J., Dasso, S., Démoulin, P., Rodriguez, L., & Janvier, M. (2016). Superposed epoch study of ICME sub-structures near Earth and their effects on galactic cosmic rays. *Astronomy & Astrophysics*, *592*, A118. https://doi.org/10.1051/0004-6361/201628571

Myllys, M., Kilpua, E. K. J., Lavraud, B., & Pulkkinen, T. I. (2016). Solar wind-magnetosphere coupling efficiency during ejecta and sheath-driven geomagnetic storms. *Journal of Geophysical Research: Space Physics*, *121*, 4378–4396. https://doi.org/10.1002/2016JA022407

Narita, Y., Glassmeier, K. H., Fornaçon, K. H., Richter, I., Schäfer, S., Motschmann, U., & Georgescu, E. (2006). Low-frequency wave characteristics in the upstream and downstream regime of the terrestrial bow shock. *Journal of Geophysical Research*, *111*, A1. https://doi.org/10.1029/2005JA011231

Osmane, A., Dimmock, A. P., Naderpour, R., Pulkkinen, T. I., & Nykyri, K. (2015). The impact of solar wind ULF Bz fluctuations on geomagnetic activity for viscous timescales during strongly northward and southward IMF. *Journal of Geophysical Research: Space Physics*, *120*, 9307–9322. https://doi.org/10.1002/2015JA021505

Russell, C. T., McPherron, R. L., & Burton, R. K. (1974). On the cause of geomagnetic storms. *Journal of Geophysical Research*, *79*(7), 1105–1109. https://doi.org/10.1029/JA079i007p01105

Shaikh, Z., Raghav, A., & Bhaskar, A. (2017). The presence of turbulent and ordered local structure within the ICME shock-sheath and its contribution to Forbush decrease. *The Astrophysical Journal*, *844*(2), 121. https://doi.org/10.3847/1538-4357/aa729f

Stone, E. C., Frandsen, A. M., Mewaldt, R. A., Christian, E. R., Margolies, D., Ormes, J. F., & Snow, F. (1998). The Advanced Composition Explorer. *Space Science Reviews*, *86*, 1. https://doi.org/10.1023/A:1005082526237

Tao, C., Sahraoui, F., Fontaine, D., de Patoul, J., Chust, T., Kasahara, S., & Retinó, A. (2015). Properties of Jupiter's magnetospheric turbulence observed by the Galileo spacecraft: Jovian magnetospheric turbulence. *Journal of Geophysical Research: Space Physics*, *120*, 2477–2493. https://doi.org/10.1002/2014JA020749

Torrence, C., & Compo, G. P. (1998). A practical guide to wavelet analysis. *Bulletin of the American Meteorological Society*, *79*(1), 61–78. https://doi.org/10.1175/1520-0477 (1998)079<0061:APGTWA>2.0.CO;2

Treumann, R. A. (2009). Fundamentals of collisionless shocks for astrophysical application, 1. Non-relativistic shocks. *The Astronomy and Astrophysics Review*, *17*(4), 409–535. https://doi.org/10.1007/s00159-009-0024-2

Tsurutani, B. T., Goldstein, B. E., Smith, E. J., Gonzalez, W. D., Tang, F., Akasofu, S. I., & Anderson, R. R. (1990). The interplanetary and solar causes of geomagnetic activity. *Planetary and Space Science*, *38*(1), 109–126. https://doi.org/10.1016/0032-0633(90)90010-N

Tsurutani, B. T., Gonzalez, W. D., Tang, F., Akasofu, S. I., & Smith, E. J. (1988). Origin of interplanetary southward magnetic fields responsible for major magnetic storms near solar maximum (1978–1979). *Journal of Geophysical Research*, *93*(A8), 8519. https://doi.org/10.1029/JA093iA08p08519

Tsurutani, B. T., Gonzalez, W. D., Tang, F., & Lee, Y. T. (1992). Great magnetic storms. *Geophysical Research Letters*, *19*(1), 73–76. https://doi.org/10.1029/91GL02783

Turc, L., Fontaine, D., Savoini, P., & Kilpua, E. K. J. (2014). A model of the magnetosheath magnetic field during magnetic clouds. *Annales Geophysicae*, *32*(2), 157–173. https://doi.org/10.5194/angeo-32-157-2014

Wilson, R. M. (1987). Geomagnetic response to magnetic clouds. *Planetary and Space Science*, *35*(3), 329–335. https://doi.org/10.1016/0032-0633(87)90159-0

Yermolaev, Y. I., Nikolaeva, N. S., Lodkina, I. G., & Yermolaev, M. Y. (2012). Geoeffectiveness and efficiency of CIR, sheath, and ICME in generation of magnetic storms. *Journal of Geophysical Research*, *117*, A00L07. https://doi.org/10.1029/2011JA017139

Zhang, G., & Burlaga, L. F. (1988). Magnetic clouds, geomagnetic disturbances, and cosmic ray decreases. *Journal of Geophysical Research*, *93*(A4), 2511–2518. https://doi.org/10.1029/JA093iA04p02511

Zhang, X. Y., & Moldwin, M. B. (2014). The source, statistical properties, and geoeffectiveness of long-duration southward interplanetary magnetic field intervals. *Journal of Geophysical Research: Space Physics*, *119*, 658–669. https://doi.org/10.1002/2013JA018937